An implicit sliding-motion preserving regularisation via bilateral filtering for deformable image registration

Bartłomiej W. Papież[a], Mattias P. Heinrich[a], Jérome Fehrenbach[b], Laurent Risser[c], Julia A. Schnabel[a]

[a] *Institute of Biomedical Engineering, Departament of Engineering Science, University of Oxford, UK*
[b] *Institut de Mathématiques de Toulouse (UMR 5219), Université Paul Sabatier, France*
[c] *Institut de Mathématiques de Toulouse (UMR 5219), CNRS, France*

Abstract

Several biomedical applications require accurate image registration that can cope effectively with complex organ deformations. This paper addresses this problem by introducing a generic deformable registration algorithm with a new regularization scheme, which is performed through bilateral filtering of the deformation field. The proposed approach is primarily designed to handle smooth deformations both between and within body structures, and also more challenging deformation discontinuities exhibited by sliding organs. The conventional Gaussian smoothing of deformation fields is replaced by a bilateral filtering procedure, which compromises between the spatial smoothness and local intensity similarity kernels, and is further supported by a deformation field similarity kernel. Moreover, the presented framework does not require any explicit prior knowledge about the organ motion properties (e.g. segmentation) and therefore forms a fully automated registration technique. Validation was performed using synthetic phantom data and publicly available clinical 4D CT lung data sets. In both cases, the quantitative analysis shows improved accuracy when compared to conventional Gaussian smoothing. In addition, we provide experimental evidence that masking the lungs in order to avoid the problem of sliding motion during registration performs similarly in terms of the target registration error when compared to the proposed approach, however it requires accurate lung segmentation. Finally, quantification of the level and location of detected sliding motion yields visually plausible results by demonstrating noticeable sliding at the pleural cavity boundaries.

Keywords: nonrigid registration, respiratory motion, sliding motion, bilateral filtering, regularisation

1. Introduction

Image registration used in a biomedical context aims to establish plausible spatial correspondences between anatomical structures in images. This task is

very challenging because deformable image registration is an ill-posed problem, and requires an additional constraint (regularization). Such regularization, in turn, highly influences the estimated deformation fields. Common regularization methods such as diffusion, elasticity or fluid methods have been derived from physical models of simple objects (Modersitzki, 2004), and thus do not usually reflect the complex underlying mechanisms (true tissue properties) of the tissue changes between the consecutive volumes. Consequently, when deformable image registration is used in a specific application, additional constraints have to be introduced. Such constraints can describe more generic displacement field properties e.g. diffeomorphism (one-to-one mappings which preserve local image topology) (Beg et al., 2005; Vercauteren et al., 2009), or local preservation of structures e.g. bones, ribs and spine stiffness (rigidity) (Staring et al., 2007; Haber and Modersitzki, 2007), tissue incompressibility (Mansi et al., 2011), volume-mass preservation (Yin et al., 2009; Gorbunova et al., 2012), or displacement field discontinuities (sliding motion) (Schmidt-Richberg et al., 2012b; Risser et al., 2013; Pace et al., 2013).

In this paper, we focus on lung motion analysis, which has been an increasingly active field of research in recent years (Murphy et al., 2011). Such methods include but are not limited to: (1) diagnosis of primary pulmonary functions such as lung ventilation quantification through analysis of local volume changes in 4D CT (Castillo et al., 2010); (2) longitudinal assessment to quantify disease and/or therapy progression e.g. measurement of tumor volume changes (tumor regression assessment) (Weiss et al., 2007) or to provide more information about changes to lungs due to chronic obstructive pulmonary disease (COPD); (3) treatment adjustment for image-guided radiotherapy (IGRT) e.g. by propagating pre-radiotherapy plans onto intra-subject radiotherapy scans to reduce normal lung irradiation (planning optimization) (Sarrut, 2006), or for accurate patient-specific estimation of differences between the prescribed and delivered doses and their impact on clinical outcome (Xing et al., 2006); (4) finally, fusion of different modality data e.g. CT and MRI for diagnosis, and equally important fusion of structural and functional imaging protocols e.g. diagnostic CT and PET/CT analysis (Baluwala et al., 2013), or protocols which are still under development for clinical usage such as correlations between hyperpolarized helium or Xenon MRI and CT for pulmonary ventilation analysis (Ding et al., 2012). An accurate lung motion compensation could also be an important tool during 4D CT lung reconstruction to improve both temporal resolution and overall reconstruction quality while reducing blurs and other motion artefacts in the reconstructed volumes. Furthermore, lung registration is an inevitable step in many approaches for forming patient-specific or cross-population motion models (Ehrhardt et al., 2011).

In general, the estimation of plausible deformations for respiratory images needs to form a compromise between smooth transformations inside organs and between groups of organs, and preserving discontinuities when multiple organs move independently. Specifically, a typical single respiratory cycle involves the action of the diaphragm, the respiratory muscles (mostly external and internal intercostal muscles), which can be further supported by the accessory respiration

muscles, and the abdominal muscles. Thus, these structures produce several local motion patterns at different locations within the thoracic cage. For example, sliding motion occurs between the pleural membranes due to the contraction of the diaphragm during normal inhale phase, which smoothly increases the volume of the thoracic cage, and hence the abdomen is moved downward. Consequently, global regularization terms cannot model local properties correctly, and more accurate models need to be considered. In order to address both the sliding and smooth motion patterns within one registration framework, various image registration approaches have been previously proposed as detailed in the following.

Most lung registration methods rely on masking (segmentation) of the lungs and adjacent organs, followed by independent registration of the segmented regions and merging of the obtained deformation fields. The segmentation can be performed for different organs: to obtain only a lung mask (Rühaak et al., 2013), the lungs and abdomen (Vandemeulebroucke et al., 2012; Delmon et al., 2013), or the lung, mediastinum and abdomen (Wu et al., 2008). While such approaches were found to be robust, they have a number of limitations. Firstly, they require an initial segmentation, which can be non-trivial to generate e.g. segmentation of the entire thoracic cage and abdomen and not only the lungs. Secondly, merging a number of different displacement fields has to be done very carefully, if this step is required for further motion analysis (especially close to any sliding boundaries). Direction dependent regularization (DDR) was proposed by (Schmidt-Richberg et al., 2012b), which decouples diffusion regularization into normal and tangential direction around the lung boundaries, based on an automatically detected masks, while the remaining part of the volume is registered using a classic diffusion model. Anisotropic diffusion regularization with the lung mask was studied for a lung phantom and CT data study in (Pace et al., 2013). Recently, Large Deformation Diffeomorphic Metric Mapping (LDDMM) (Beg et al., 2005) was extended towards a piecewise-diffeomorphic registration that enables explicit sliding motion modeling (Risser et al., 2013). Although a very accurate domain splitting strategy has to be provided to ensure a piecewise-diffeomorphism, a composition of local estimates of the deformation field is done efficiently through parameterization via the velocity field, making this method mathematically sound.

For approaches where no segmentations are available or possible to obtain, sliding motion can be approximated by spatially varying regularization based on local properties of the tissue (e.g. derived directly from Hounsfield units if CT data are available). However, the estimated deformations can still remain smooth at lung boundaries (thus underestimating sliding motion especially near to boundaries). Applying discontinuity preserving regularisation across the entire volume domain, as in (Ruan et al., 2009; Heinrich et al., 2010), does not distinguish between different organs, producing artificial sliding motion. Locally adaptive regularization has also been used to enforce the rigidity on some volume objects e.g. chest ribs and spine. The most related method to the one presented in this paper was proposed by Staring et al. (2007). This method is based on an iterative procedure of adaptive filtering (averaging) of the deforma-

tion field that is applied over the region of each rigid object. Another example is the recent work by (Baluwala et al., 2013), where a fluid registration framework with preservation of topology, displacement discontinuity, and rigidity is proposed. However, that method also relies on the segmentation of the lung surface and bony structures.

In our work we explore the use of the bilateral filter, widely used in computer vision applications due to its simplicity and effectiveness, for its utility in lung registration with sliding motion. The bilateral filtering presented by (Tomasi and Manduchi, 1998) forms a non-linear diffusion technique for image de-noising, taking into account not only local spatial smoothness (as e.g. when using (an)isotropic Gaussian filters), but also local intensity (dis)similarities. By reducing the influence of pixels that have different intensity values, edges are preserved in the image. In the same spirit, an optical-flow based framework was proposed that extends the usability of bilateral filters for motion estimation in the presence of occlusions in video sequences (Xiao et al., 2006; Sand and Teller, 2008). Occlusion detection is different from sliding motion estimation which can be observed at the boundaries of the pleural cavity, but its main objective is to minimise *information exchange* between certain objects of interests e.g. by handling discontinuity of the estimated displacement field.

In our previous work (Papiez et al., 2013), we presented initial results obtained by a novel automated registration framework by integrating adaptive bilateral filters to regularise estimated deformation fields. For this purpose, we replaced the classic Gaussian kernel used to regularize the estimated deformation field in the Demons framework (Thirion, 1998) by a new kernel that is dependent on anisotropic diffusion (based on the local structure tensor), as well as on the intensity and deformation dissimilarity. As was shown, the proposed regularization model does not require an explicit segmentation prior incorporated into the Demons deformable registration to preserve discontinuous deformation fields at the sliding boundaries. Here, we extend this work fourfold: (1) we handle the intensity changes caused by air compression in the lungs by using local CT volume representations via normalized gradient fields (NGF) (Haber and Modersitzki, 2006) and incorporate them into a vector-valued Demons framework; (2) we provide a theoretical and experimental analysis of the application to CT lung motion estimation; (3) we perform an extensive quantitative and qualitative validation using two 4D CT data sets consisting of synthetically generated examples and clinical cases of 10 patients with esophageal and lung cancer, and finally (4) we quantify the level and location of detected sliding motion using the maximum shear stretch criterion (Amelon et al., 2013).

This paper is structured as follows. Section 2 first briefly presents Demons, a classic non-linear image registration formulation with a common diffusion regularization (2.1). Then, a novel normalized gradient field based Demons registration is formulated (2.2). Finally, this section finishes with a description of an adaptive bilateral filtering based regularization (in Sec. 2.4), which extends the classic Gaussian smoothing procedure which is briefly described in Sec. 2.3. The new regularization model consists of three basic components: spatial variability, local intensity differences, and the local deformation field similarity to

deal with complex organ motion estimation. In Sec. 3 an example of the specific application of the developed technique to lung motion estimation is presented and discussed in detail together with the parameter choices. Sec. 4 presents the lung data sets used for testing and evaluating the new lung motion correction methods, and summarizes and discusses the results. These results are compared to recently published methods from the literature. Based on the presented results, we show that our framework is capable of achieving similar results to algorithms that require a prior knowledge from segmentation, whilst preserving sliding motion. The paper ends with a discussion and conclusions given in Sec. 5.

2. Demons registration

This section presents the classic diffusive registration model solved using a Demons framework (Thirion, 1998; Vercauteren et al., 2009), and then describes our new approach based on Demons, which is able to handle complex sliding motion problems.

2.1. Image registration via Demons framework

In this work, pair-wise image registration of a moving image I_m to a fixed image I_f is encoded in a dense deformation field $\vec{u}$. We denote $I_m(\vec{u}) = I_m \circ \vec{u}$ the deformed (moving) image. A generic non-rigid registration framework can be formulated as follows:

$$\arg\min_{\vec{u}} \left(E(\vec{u}) = Sim(I_f, I_m(\vec{u})) + \alpha Reg(\vec{u})\right) \tag{1}$$

where $E(\vec{u})$ is a global energy to be optimised, combining a similarity of the input images $Sim(I_f, I_m(\vec{u}))$ and a regularisation term $Reg(\vec{u})$. This work uses the Demons approach (Vercauteren et al., 2009), which is a widely used non-parametric registration framework, where in the original version the similarity $Sim(I_f, I_m(\vec{u}))$ is formulated as the sum of squared intensity differences (SSD) $\frac{1}{2}\|I_f - I_m(\vec{u})\|^2$ and a diffusion based regularisation $Reg(\vec{u}) = \|\vec{u}\|^2$ of the deformation field is performed by Gaussian smoothing.

2.2. Demons registration using Normalized Gradient Fields

Usage of SSD based image registration implies an assumption that the corresponding structures in both input images have constant intensity values. However, this assumption is violated in the case of CT lung data, which commonly change intensity values due to density changes associated with inflation and decompression (Yin et al., 2009). Similarity terms measuring a global intensity relationship such as point-based cross-correlation or mutual information for deformable registration (Hermosillo et al., 2002) cannot capture those subtle changes because of their local nature across different parts of the lung (see results in (Heinrich et al., 2012)). For this purpose, we propose here to evaluate the concept of normalized gradient fields (NGF) as a local image descriptor,

which can be used to resolve local intensity variations. NGFs were originally introduced by Haber and Modersitzki (2006) to handle deformable registration of multi-modal images because of being better suited for optimization than mutual information and its variations. The NGFs of any image I_l at any spatial position $\vec{x}$ are defined as:

$$\vec{F}^l(\vec{x}) = \vec{F}(I_l(\vec{x})) = \frac{\nabla I_l(\vec{x})}{\|\nabla I_l(\vec{x})\|_\epsilon}\,, \tag{2}$$

where $\|\nabla I_l(\vec{x})\|_\epsilon = \sqrt{\nabla I_l(\vec{x})^T \nabla I_l(\vec{x}) + \epsilon}$ homogenizes the NGF in areas with different intensity gradients, and does not emphasize the gradients generated by intensity differences having an amplitude lower than ϵ intensity units. The original Demons is formulated for scalar-valued images, while the NGF is a vector-valued representation. Therefore, following (Peyrat et al., 2010), we use the linearisation of differences between vector-valued descriptors $\vec{F}(I_f) - \vec{F}(I_m)$ that was proposed for the multichannel Demons. The detailed description with detailed mathematical derivations of the presented registration framework can be found in (Vercauteren et al., 2009) for scalar-valued images, and in (Peyrat et al., 2010) for vector-valued functions.

2.3. Demons registration with anisotropic Gaussian smoothing

In the Demons algorithm, diffusion regularisation is performed by smoothing the deformation field $\vec{u}$ using an isotropic Gaussian kernel G_{iso} at each iteration:

$$\vec{u}_{new}(\vec{x}) = G_{iso} * (\vec{u}_{old}(\vec{x}) \circ \vec{du}(\vec{x})) \tag{3}$$

where $\vec{u}_{new}$ is the new estimate of the deformation field, $\vec{u}_{old}$ is the deformation field calculated in the previous iteration, and $\circ$ is a composition operation. One can replace the isotropic Gaussian kernel G_{iso} by an anisotropic diffusion kernel G_{ani} which varies at different image positions $\vec{x}$ with respect to an image structure tensor $\vec{D}$ (Tschumperle and Deriche, 2005; Xiao et al., 2006). The image structure tensor $\vec{D}(\vec{x})$ for n-dimensional volumes is defined as (Hermosillo et al., 2002):

$$\vec{D}(\vec{x}) = \frac{(\beta + \|\nabla I(\vec{x})\|^2)\vec{Id} - \nabla I(\vec{x}) \nabla I(\vec{x})^T}{(n-1)\|\nabla I(\vec{x})\|^2 + n\beta} \tag{4}$$

where β is an anisotropy parameter and $\vec{Id}$ is the $n \times n$ identity matrix. As can be expected, if the intensity values around point $\vec{x}$ are (close to) constant ($\|\nabla I(\vec{x})\| \approx 0$), all eigenvalues of $\vec{D}$ have the same value and the kernel G_{ani} is equivalent to an isotropic kernel G_{iso}. A review of anisotropic diffusion filtering techniques can be found in (Weickert et al., 1998).

2.4. Demons registration with adaptive bilateral smoothing

In order to prevent the deformation field to be smoothed across object boundaries, which would not be physically realistic, we propose to replace the

standard Gaussian filtering of the deformation field by a more advanced non-linear filtering technique originally proposed for image denoising (Tomasi and Manduchi, 1998). The bilateral filter smoothes an input image $I_{old}(\vec{x})$ using two combined Gaussian kernels in the following way:

$$I_{new}(\vec{x}) = \frac{1}{W(\vec{x})} \sum_{\vec{y}\in\mathcal{N}(\vec{x})} \underbrace{\exp\left(-\frac{(\vec{x}-\vec{y})^T(\vec{x}-\vec{y})}{2\sigma_{\vec{x}}^2}\right)}_{G_{\vec{x}}(\vec{x},\vec{y})} \underbrace{\exp\left(-\frac{\|I_{old}(\vec{x})-I_{old}(\vec{y})\|^2}{2\sigma_r^2}\right)}_{G_r(I(\vec{x}),I(\vec{y}))} I_{old}(\vec{y}) \tag{5}$$

where G_{iso} is a Gaussian kernel of variance $\sigma_{\vec{x}}^2$ defined on the spatial domain, and G_r is another Gaussian kernel of variance σ_r^2 defined on the intensity domain I_{old} instead of the spatial domain. Locations $\vec{y}$ are also considered in the spatial neighbourhood $\mathcal{N}(\vec{x})$ of $\vec{x}$, and $W(\vec{x})$ is a normalisation factor for this image neighbourhood.

By extending this bilateral filtering strategy to deformation fields, and not only image intensities, we can rewrite the regularisation scheme (Eq. (3)) as:

$$\vec{u}_{new}(\vec{x}) = G_x G_r * (\vec{u}_{old}(\vec{x}) \circ \vec{du}(\vec{x})) \tag{6}$$

Finding a balance to quantify to what extent intensity differences are related to sliding motion can be particularly difficult in medical images.

If the size of the kernel σ_r^2 is too small, the deformation field is over-segmented, *i.e.* each intensity change in the image (within a range of σ_r^2) leads to artificial deformation field discontinuities in the whole image domain. In the opposite case, if σ_r^2 is too high, the results are similar to those estimated using only G_{iso} and do not model any sliding motion pattern. In addition to this, some organs have very similar intensity values, although they can slide along each other. Therefore, we use a supplementary kernel (Xiao et al., 2006) and the original bilateral filtering for deformation fields is extended in the following way:

$$\vec{u}_{new}(\vec{x}) = \frac{1}{W(\vec{x})} \sum_{\vec{y}\in\mathcal{N}(\vec{x})} G_{iso}(\vec{x},\vec{y}) G_r(I(\vec{x}),I(\vec{y})) \underbrace{\exp\left(-\frac{(\vec{u}_{old}(\vec{x})-\vec{u}_{old}(\vec{y}))^T(\vec{u}_{old}(\vec{x})-\vec{u}_{old}(\vec{y}))}{2\sigma_{\vec{u}}^2}\right)}_{G_{\vec{u}}(\vec{u}(\vec{x}),\vec{u}(\vec{y}))} \vec{u}_{cur}(\vec{y}) \tag{7}$$

where $G_{\vec{u}}$ describes a Gaussian kernel based on the local deformation field dissimilarity and $\vec{u}_{cur}(\vec{x}) = \vec{u}_{old}(\vec{x}) \circ \vec{du}(\vec{x})$. The new kernel G_u reduces the influence of deformation field smoothing based on the local properties of the deformation field. Using this new kernel, the proposed filtering procedure can effectively exclude information from structures having different intensities and deformation

field patterns, hence maintaining both continuous and discontinuous deformations in the image domain, and avoid *motion over-segmentation* which is typical for image-driven regularisation (Zimmer et al., 2011). The overall structure of the presented registration framework is summarized in Algorithm 1. We further discuss the tuning of the three kernels G_{iso}, G_r, and $G_{\vec{u}}$ when applied to lung data registration in Sec 3.

Algorithm 1 NGF-Demons with bilateral filtering

Input: Images: I_f and I_m Parameters: $\sigma_{\vec{x}}$, σ_r and $\sigma_{\vec{u}}$
Output: Displacement field $\vec{u}_{new}$

$\vec{u}_{new} := \vec{0}$
$i = 0$
repeat
    $\vec{u}_{new} := \vec{u}_{old}$
    Compute the update $\vec{du}$
    Update the deformation field $\vec{u}_{cur} := \vec{u}_{old} \circ \vec{du}$
    Compute $\vec{u}_{new}$ by filtering $\vec{u}_{cur}$ using Eq. (7)
    Increment the iteration index i
until (convergence of $||\vec{u}_{new} - \vec{u}_{old}||_2^2$) **or** ($i \geq IterMax$)
return $\vec{u}$

2.5. Convergence

In this section, we present how the convergence of Algorithm 1 is reached. This convergence is not straightforward as the smoothing kernel of Eq. (7) evolves iteration after iteration. We therefore present Algorithm 1 as a continuous model, to make it mathematically clear, and then discuss its convergence. We note $I(\vec{x},t) = I_m(\vec{x}+\vec{u}(\vec{x},t))$, where the time t is a continuous representation of the iteration index. The continuous model can be formulated as:

$$\begin{cases} \dfrac{\partial \vec{u}}{\partial t}(\vec{x}) &= \alpha \vec{du} + \int_{\vec{y}\in\mathcal{N}(\vec{x})} G(\vec{x},\vec{y})\vec{u}(\vec{y},t)d\vec{y} - \vec{u}(\vec{x}) \\ \dfrac{\partial I}{\partial t}(\vec{x}) &= \nabla I \cdot \dfrac{\partial \vec{u}}{\partial t}\,, \end{cases} \tag{8}$$

where: $G(\vec{x},\vec{y}) = \frac{1}{W(\vec{x})} \exp\left(-\frac{||\vec{x}-\vec{y}||^2}{2\sigma_{\vec{x}}^2} - \frac{|I(\vec{x},t)-I(\vec{y},t)|^2}{2\sigma_r^2} - \frac{|\vec{u}(\vec{x},t)-\vec{u}(\vec{y},t)|^2}{2\sigma_{\vec{u}}^2}\right)$ and $W(\vec{x})$ equals $\int_{\vec{y}\in\mathcal{N}(\vec{x})} G(\vec{x},\vec{y})d\vec{y}$. Convergence of $\vec{u}(\vec{x})$ is reached if $\partial\vec{u}/\partial t = 0$ for all $\vec{x}$. We then have the following property:

$$\vec{u}(\vec{x}) = \alpha \vec{du} + \int_{\vec{y}\in\mathcal{N}(\vec{x})} G(\vec{x},\vec{y})\vec{u}(\vec{y},t)d\vec{y}\ ,\ \forall \vec{x} \in \Omega \tag{9}$$

As in most image registration algorithms, an equilibrium is obtained between the displacement field $\vec{u}$ and the sum of the *update forces* (1^{st} term) plus the *smoothing forces* (2^{st} term). Importantly, the filter kernel $G(\vec{x},\vec{y})$ is non-stationary and depends on the deformed image $I(\vec{x},t)$ as well as the displacement field $\vec{u}(\vec{x},t)$. However, the equilibrium of Eq. (9) involves that $\partial\vec{u}/\partial t = 0$ by definition. Following the second relation of Eq. (8) we also have: $\partial I/\partial t = 0$. As a consequence, $G(\vec{x},\vec{y})$ is also stable. To conclude, the non-stationarity of $G(\vec{x},\vec{y})$ makes the system Eq. (8) non-linear but still allows its convergence.

Parameters $\{\sigma_{\vec{x}},\sigma_r,\sigma_{\vec{u}}\}$ have however a strong influence on the local properties of the deformations at convergence. We discuss these properties hereafter by relating them to the specific problem of lung registration without segmentation of the thoracic cage. In this context, we give a clear strategy for selecting the parameters $\{\sigma_{\vec{x}},\sigma_r,\sigma_{\vec{u}}\}$ of $G(\vec{x},\vec{y})$.

3. Application to lung registration

In this section we focus on the particular application of our framework presented in the previous section to respiratory motion estimation. The lungs are sliding along the surrounding organs during the respiratory cycle, thus, leading to discontinuous deformations at the pleural cavity boundaries whilst causing smooth deformations inside. Therefore, we consider the typical regions in the registered images of the lungs $I(x,t)$ ($\approx I_m(x+u(x,t))$) in terms of the local tissue and deformation field properties. These regions are illustrated in Fig. 1 and represent the following properties subdivided in two groups, based on intensities difference: (R1) deformable structures, (R2) compressible structures, and (R3) rigid structures; and based on intensities and deformation difference: (R4) smooth deformation field of the entire structure, (R5) smooth deformation field between different structures and (R6) discontinuous deformation field between neighbourhood structures. Additionally, we highlight three commonly distinguishable examples of local intensity levels and deformation fields configurations of the thoracic cage where the behaviour of the kernel $G(\vec{x})$ is remarkably different at each spatial position $\vec{x}$. The regions R4, R5, and R6 are related to the configurations shown in Fig. 1: (R4) is within the lungs with a smooth deformation field, (R5) contains the lower (inferior) part of the lungs and abdomen with a relatively smooth deformation field, (R6) is the sliding interface between the pleural cavity and chest wall, where the largest amount of sliding motion can be observed. We recall that the proposed registration is designed to preserve sharp sliding motion only in regions like (R6).

Case 1: Homogeneous intensity regions and homogeneous displacement field. Consider a region of constant intensities ($\|\nabla I(\vec{x}\| \approx 0$)), *i.e.* a region where the importance of the regularisation term $G_{\vec{x}}$ (which contains spatial smoothness $\sigma_{\vec{x}}$) is significantly higher than the two other kernels. In such case, G is equivalent to a standard Gaussian kernel and the associated PDE to solve can be related to the heat equation with moving sources. Therefore, the registration algorithm is locally a classic optical flow / demons like registration with an isotropic diffusion

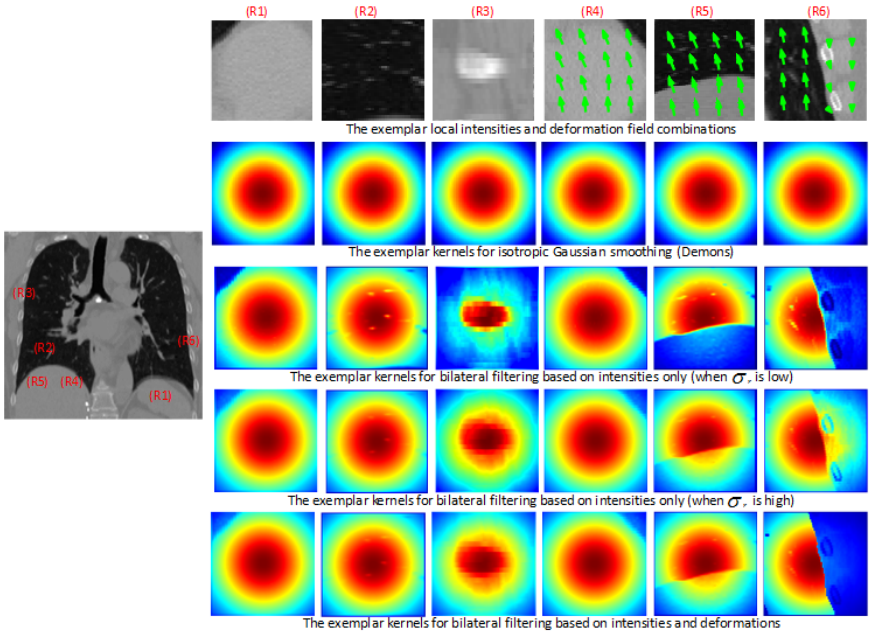

Figure 1: Comparison between different kernels used for deformation filtering: the isotropic Gaussian kernels G_{iso}, the only intensities difference based bilateral kernels $G_{iso} \cdot G_r$ with both low and high value of σ_r, and the presented bilateral filtering kernels incorporating intensities and deformation fields difference $G_{iso} \cdot G_r \cdot G_{\vec{u}}$. The notable examples of different tissue properties based on the local intensities (Hounsfield units): (R1) deformable structures, (R2) compressible structures, and (R3) rigid structures; and the notable examples of combination between local intensities $I(\vec{x})$ and deformation fields $\vec{u}(\vec{x})$ (green arrows) that can occur in respiratory image registration: (R4) constant intensities and smooth deformation field, (R5) intensity changes related to organs boundaries and smooth deformation field, and (R6) intensity changes related to organs boundaries with discontinuous deformation field (sliding motion). On the left, coronal plane of a CT lung volume with the depicted regions of interest where the local properties of kernels for deformation field filtering $G(\vec{x})$ are different. The proposed composition of three kernels $G_{iso} \cdot G_r \cdot G_{\vec{u}}$ produces kernels which visually have better overlap with the underlying anatomical structures.

regularisation. Parameters of G should be tuned so that this case is observed in regions like (R4).

Case 2: Regions with high intensity gradients and homogeneous displacement field. Now consider that the regularisation term G_r (where a value of σ_r differentiates locally dissimilar intensities) has the strongest influence in the close neighbourhood of $\vec{x}$. This should be the case where a displacement field $\vec{u}$ presents locally small variability, and intensity differences are significant ($\|\nabla I(\vec{x})\| \gg 0$). In Fig. 1, this configuration of intensities and deformation field will be typically found in region (R5). To some extent, it will also be observed in region (R6) if there is no or only little sliding motion, for example during the first iterations of the computations in all cases (because the displacement field is usually

initialised by an identity deformation $\vec{u} = \vec{Id}$). There, in the region (R6), we would like most of the smoothing to be performed either inside or outside the lungs. Little information exchange will also be made through the lung boundary to capture the up and down motion in region (R5) or to allow a limited motion of normal to the lung boundary in (R6). At the start of the registration, this will also allow to capture eventual sliding motion in regions like (R6). The deformation will however be smoothed there due to the limited amount of information exchange through the lung boundaries; thus another kernel is required to effectively distinguish between sliding and non-sliding cases. We will see that the third term can enhance these discontinuities.

Case 3: Regions with high intensity gradients and heterogeneous displacement field. Finally, we consider the last part of the regularisation term $G_{\vec{u}}$ (which reduces the inference of locally dissimilar motion through adjustment of value $\sigma_{\vec{u}}$) with the locally strongest influence. As discussed for Case 2, this will typically happen in regions like (R6) where a discontinuity has already been captured. This corresponds to the configuration in the right column (R6) of Fig. 1. The discontinuity captured in Case 2 is however relatively smooth and has to be sharpened to look physiologically plausible. This will occur if $\sigma_{\vec{u}} < |\vec{u}(\vec{x},t) - \vec{u}(\vec{y},t)|$ for pairs of points $\vec{x}$ and $\vec{y}$ at a distance lower than $\sigma_{\vec{x}}$. The third term is then a discontinuity enhancement term.

Summary of selection of $\sigma_{\vec{x}}$, σ_r and $\sigma_{\vec{u}}$ for CT lung data. This section summaries our experimental results to select optimal parameters $\sigma_{\vec{x}}$, σ_r and $\sigma_{\vec{u}}$ for CT lung data. The parameter selection of $\sigma_{\vec{x}}$, σ_r and $\sigma_{\vec{u}}$ is related to the discussions above:

Spatial smoothness $\sigma_{\vec{x}}$: As in other diffusion based registration algorithms, the distance $\sigma_{\vec{x}}$ should be sufficiently large to smooth the sparse features observed inside and outside of the lungs, but not too large to capture local deformations. In this study, we found that $\sigma_{\vec{x}} = 3.0mm$ produces the best results for lung CT data registration.

Intensities difference σ_r: The intensity difference σ_r should be similar to the difference between the average intensity in the lungs and the average intensity of the tissues around the lungs. In this work, we found that $\sigma_r = 310$ [Hounsfield units] works well for lung CT data registration.

Deformation field difference $\sigma_{\vec{u}}$: The deformation magnitude $\sigma_{\vec{u}}$ should be larger than the difference of deformation magnitude captured between points at a distance lower than $\sigma_{\vec{x}}$ everywhere, except around the pleural cavity, where $\sigma_{\vec{u}}$ should be lower than this magnitude. This term is therefore difficult to select. To avoid motion over-segmentation, we set it so that it only captures sharp discontinuities when a large amount of sliding motion is observed. For instance, if we consider that 20mm is a large amount of sliding motion, we can select $\sigma_{\vec{u}}$ as equal to 5mm.

4. Validation

4.1. Materials

We assessed the proposed approach, the NGF based Demons with a regularisation performed via bilateral filtering procedure, on two publicly available 4D CT respiratory image data sets.

The first data set consists of a set of synthetically generated but anatomically realistic 4D CT volumes modelling consecutive respiratory phases created using the 4D NURBS-based Cardiac-Torso (NCAT) phantom (Segars, 2001). The size of the data is $192 \times 192 \times 192$ with a spatial resolution of $2.0 \times 2.0 \times 2.0 mm^3$. For each volume, segmentation labels for lungs, liver, and ribs are easily obtained by thresholding with some minor manual corrections as these volumes have a limited number of intensity levels.

For the second part of the validation, we used the *Dir-Lab*[1] data set which consists of planning 4D CT volumes acquired from ten patients treated for oesophageal and lung cancer (Castillo et al., 2009). The spatial resolution of that data varies between $0.97 \times 0.97 \times 2.5 mm^3$ and $1.16 \times 1.16 \times 2.5 mm^3$. The first five cases included in this data set (denoted here *c1-c5*) are cropped to include the entire rib cage and further subsampled to form an in-plane dimension of 256×256. We apply a similar cropping procedure to the remaining five cases (*c6-c10*), but no subsampling was performed. This is only done to improve computational speed, and does not otherwise affect the registration behaviour. Each *Dir-Lab* volume includes 300 landmarks manually identified by experts. The target registration error (TRE) was evaluated as a measure of registration accuracy. The landmarks are well distributed throughout the entire lung chest, including landmarks located close to the pleural cavity boundaries, and the intra-observer error is approximately $1.0 mm$ (Castillo et al., 2009). All data sets used in the following experiments are already globally aligned, therefore no pre-alignment registration was performed. For each case, the end-of-inspiration volume was chosen as a reference, and the end-of-expiration volume as a moving image.

4.2. Experimental setup

The presented similarity measure (difference between normalised gradient fields) and regularisation procedure (based on bilateral filtering with supplementary kernels) were incorporated into a Demons registration framework (Thirion, 1998). We implemented the Demons using an update composition scheme with a fixed maximal update step of one voxels (see Vercauteren et al., 2009, for details) together with four resolution levels. Within this framework we compared the Demons with the new NGF based similarity measure (denoted by **ngf**) against the traditional SSD (denoted by **ssd**). The NGF image representation was recalculated in each iteration from the warped image to preserve correct orientation of the NGF vectors. To compare the regularisation methods, a

[1] These data are made publicly available on http://www.dir-lab.com

quantitative evaluation was performed using four different kernels for filtering the deformation field: (1) spatially isotropic Gaussian G_{iso} (**iso-ssd** and **iso-ngf**) denoting these as the the classic SSD Demon (Thirion, 1998), and the proposed NGF based Demon methods, respectively. (2) spatially anisotropic Gaussian G_{ani} (**ani-ssd**, and **ani-ngf**) based on the image structure tensor $\vec{D}$ (given in Eq. (4)), (3) the presented bilateral kernel with an isotropic Gaussian on spatial, intensity and deformation similarity components $G_{iso}G_rG_{\vec{u}}$ (**ibil-ssd** and **ibil-ngf**), and (4) a spatially anisotropic Gaussian together with intensity and deformation similarity components $G_{ani}G_rG_{\vec{u}}$ (**abil-ssd** and **abil-ngf**).

Additionally, we performed the Demon registration using a spatially isotropic Gaussian G_{iso} (**iso-ssd** and **iso-ngf**) with masked region of interests. This is to compare our fully automated framework, which does not require masking of regions such as the lungs, with the more commonly used lung registration approaches working on the lung regions only. We used two types of masks: (1) (**lg-ssd** and **lg-ngf**) *lung mask* generated using a very accurate lung tissue segmentation algorithm presented in (Lassen et al., 2011). This particular choice was motivated by the results achieved for the EMPIRE10 lung registration challenge for the algorithm using these masks (Rühaak et al., 2013). Because of removing tissue outside the rib cage, the sliding motion problem is entirely avoided. (2) (**mm-ssd** and **mm-ngf**) The second masking approach *motion mask* splits the image domain into two regions, one with significant motion (the inner thorax cage) and one which is less moving (the outer thoracic region) (Vandemeulebroucke et al., 2012; Risser et al., 2013). During the experiments using masks, we set the intensity values of the non-masked region to the maximum of the ones inside the masked region following (Heinrich et al., 2013). In most cases, the registration with a bilateral filter without deformation similarity kernel $G_{iso} \cdot G_r$ produces unrealistic deformation fields, thus the quantitative results obtained are not included.

The quantitative evaluation of the registration results was further assessed by performing a two-sample Wilcoxon rank sum test between each pair of estimated landmarks for the originally proposed registration method (**ibil-ssd**) and the other currently evaluated methods.

The presented experiments both on the synthetic NCAT phantom and on the *Dir-Lab* data sets are a more advanced extension to our previous work (Papiez et al., 2013) and include (1) comparison to the approaches with different types of masks (lung mask, and motion mask), (2) comparison between the classic Demons and the NGF-based Demons algorithm, (3) quantitative analysis of the sliding motion for the presented algorithms for the 4D CT lung image registration, and (4) comparison to recently published works on sliding motion estimation. The minor improvements of the results compared to our previous work are due to the upgrades introduced into our software and a very extensive search over the parameter space that has been carried out for each method.

The best design parameters ($\sigma_{\vec{x}}$, σ_r, $\sigma_{\vec{u}}$, β) were determined empirically by an extensive search over a sufficiently large parameter space for each method separately using two volumes labelled *c6* and *c9* (which exhibit relatively large

displacements) from the *Dir-Lab* data set, from which we chose the parameters that gave the smallest target registration error. These were then fixed for all experiments (for both the NCAT phantom data set and the Dir-Lab set) as discussed in Section 3. The parameters are as follows: $\sigma_{\vec{x}}$ = 3mm, σ_r=310 [Hounsfield units], $\sigma_{\vec{u}}$=5mm, β=0.1. All resulting deformation fields have a positive value of the determinant of Jacobian, indicating that there is no implausible folding of the deformation field.

4.3. Quantification of estimated deformation fields

NCAT phantom data

Table 1: Average Dice coefficient (DICE) obtained for the NCAT phantom data set using the Demons framework with four different filtering kernels. No statistical significance of improvement (p-value>0.05) between **ibil-ssd** compared to others methods was found despite the better results on average for the new methods. The methods which use the additional bilateral filter kernels achieve higher DICE than the conventional Demons algorithm.

	DICE (avg ± std)				
	before	**iso-ssd**	**ani-ssd**	**ibil-ssd**	**abil-ssd**
lungs	81.49±10.0	93.54±4.3	94.31±3.6	96.90±1.2	96.49±1.6
liver	75.52±12.2	90.25±7.7	90.97±7.1	91.67±5.9	91.53±6.1
ribs	67.00±13.9	85.61±2.5	85.61±2.3	88.91±0.8	88.21±0.8
spine	91.19± 1.5	90.87±1.7	90.81±1.7	91.16±1.3	91.15±1.4

In this section, we present the results of evaluation for the proposed approach using the NCAT phantom data. We generated volumes representing different states of the respiratory cycle starting from the end of the inspiration through the intermediate stages to the end of the expiration. Although these images consist of few intensity levels only, this does not affect the real organ motion estimation in practice. However, it makes deformable registration more challenging and entirely linked to the particular regularisation model, as the registration forces in the areas of constant intensity values are directly influenced by the chosen regularisation.

An exemplary coronal view of the NCAT phantom data together with the estimated deformation field used for quantitative evaluation is shown in Fig. 2.

The registration accuracy was assessed by the Dice coefficient ($DICE = (2|A \cap B|)/(|A| + |B|)$) calculated separately for each organ of interest (lungs, liver, ribs and spine) between ground truth labels (A) provided in the phantom data and segmentations obtained from registration via label propagation (B). The registration results on the NCAT phantom are presented in Tab. 1. As shown in Tab. 1, the DICE exhibits an improvement for methods based on bilateral filtering (**ibil-ssd** and **abil-ssd**) when compared to both methods using isotropic and anisotropic Gaussian smoothing (**iso-ssd** and **ani-ssd**). However, these differences are not statistically significant. This phantom example highlights also the differences between the evaluated regularisation models in terms

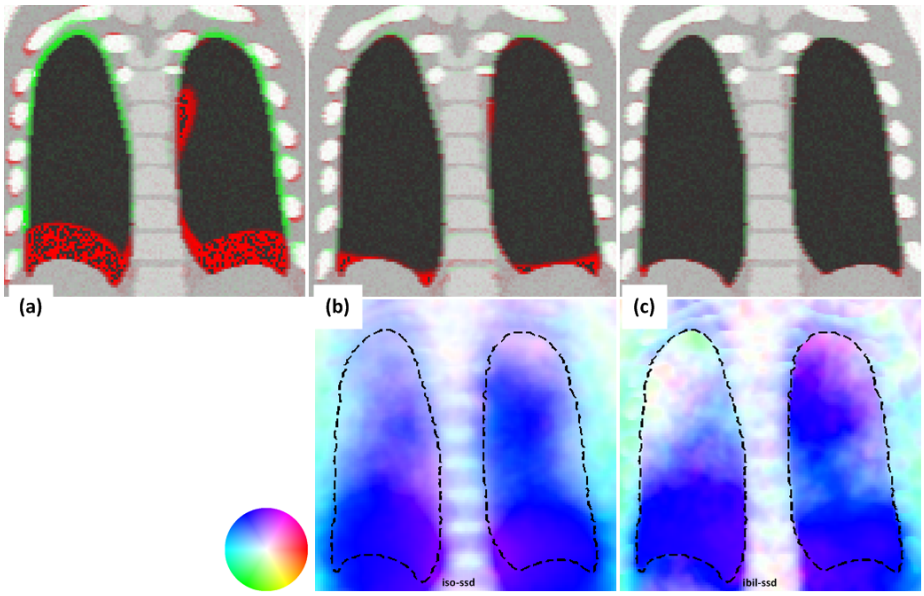

Figure 2: Qualitative registration results for phantom volumes of the NCAT data set. The top row shows the coronal view of the reference image with the corresponding overlap of exhale image (red and green) while the bottom row shows the coronal view of the colour coded representation of deformation field vectors (in HSV colour space). In columns from left to right: (a) before registration; (b) Demons with isotropic Gaussian kernel (**iso-ssd**), (c) the proposed Demons with supplementary bilateral kernels (**ibil-ssd**) While all methods produce visually similar outcomes, registration using **ibil-ssd** slightly improves registration accuracy especially close to the lung boundary.

of the anatomical correspondence and deformation fields plausibility. The classic Demons algorithm smoothly propagates the estimated deformation field outside of the rib cage by performing Gaussian filtering of deformation field. In contrast to that, the methods based on the presented bilateral filtering procedure (**ibil-ssd** and **abil-ssd**) do not smooth the deformation field across the lung and the rib cage boundaries, leading to higher DICE values for the surrounding organs. In summary, implicit modelling of sliding motion during registration on the synthetic NCAT data improves the registration results when compared to the state-of-the-art Demons algorithm.

Dir-Lab CT data

In this section, we report the results of the quantitative and qualitative analysis performed using the clinical *Dir-Lab* data set. For each pair of volumes (maximal inhale and exhale scans of the same patient), an average distance between 300 landmarks after registration was calculated with results shown in Tab. 2, and in Tab. 3 for Demons based on the classic SSD force, and for the NGF based Demons, respectively. For comparison purposes, the TREs obtained before registration are also given in Tab. 2 with an average TRE

for all 10 cases of $8.46 \pm 5.4mm$. Examples of the registration outcomes for the inhale-exhale case $c5$ from *Dir-Lab* using classic SSD Demons (**iso-ssd**), the NGF-based Demons with Gaussian smoothing (**iso-ngf**) and the method consisting of NGF-based Demons and bilateral filtering procedure (**ibil-ngf**) along with the magnitudes and vector representation of the deformation fields are shown in Fig. 3 and Fig. 4, respectively. All methods produce a statistically significant improvement (p-value¡0.05) in terms of TRE compared to before registration. We found that in both cases, when using classic Demons, and the NGF-based Demons, the methodologies using bilateral filters procedure for deformation field smoothing achieved a lower target registration error (TRE) than when using Gaussian smoothing alone. In particular, the methods with isotropic Gaussian bilateral filters achieve the lowest TRE ($2.11 \pm 0.9mm$ for **ibil-ssd**, $1.95 \pm 0.7mm$ for **ibil-ngf**) which is lower than the spatial resolution of the CT data. Additionally, we compared these results with the approaches that use masks to avoid the problem of sliding motion estimation. The methods using lung masks produce a slightly lower TRE ($2.05 \pm 0.8mm$ for **lg-ssd**, $1.93 \pm 0.7mm$ for **lg-ngf**) but no statistical significance was found between **ibil-ssd** and **ibil-ngf**, respectively. In contrast, the methods using motion masks achieve slightly higher TRE ($2.14 \pm 0.9mm$ for **mm-ssd**, $2.06 \pm 0.8mm$ for **mm-ngf**), and a statistical significance was also not found compared to **ibil-ssd** and **ibil-ngf**, respectively.

Furthermore, the quantitative results given in Tab. 2 and in Tab. 3 are consistent with the visual inspection of the deformation fields shown in Fig. 3 and Fig. 4. The classic Demons method does not preserve discontinuities at the lung boundaries, hence the displacement field smoothly changes the magnitude and direction across those boundaries (see zoomed images in Fig. 5). In contrast, the displacement field estimated by the proposed method **ibil-ngf** clearly indicates the two preferable properties at the pleural cavity boundaries: discontinuities between rib cage and lungs, and smooth deformations at the lung and abdominal cavity interface.

4.4. Quantification of similarity measures

We also assess the vector-valued version of Demons based on the Normalized Gradient Fields representation for volumetric medical CT data. The results presented in Tab. 2 and Tab. 3 also indicate that the Demons registration forces derived from the Normalized Gradient Fields representation of CT volumes produce lower TRE when compared to the classic SSD Demon forces.

The Demons using a vector-valued normalized gradient fields instead of intensity values show clear improvements for CT data registration. In particular, the average TRE was reduced from $2.71 \pm 1.9mm$ for **iso-ssd** to $2.35 \pm 1.5mm$ for **iso-ngf** yielding $0.36mm$ improvement. The improvement is less remarkable for approaches using the proposed regularization based on bilateral filtering and for approaches using both types of mask, with an average improvement of $0.16mm$ for **ibil-ngf** and $0.12mm$ for **lg-ngf**. These results suggest that the normalized gradient fields can better capture the appearance changes between inhale and exhale scans. Visual inspection of the deformation field properties

Table 2: Average target Registration Error (TRE) and standard deviation obtained for the Dir-Lab data set using the classic Demon forces with four different filtering kernels (between 3rd (**iso-ssd**) and 6th column (**abil-ssd**)) and for the Demons with the isotropic Gaussian kernel (**iso-ssd**) with two different masks (last two columns). The proposed **ibil-ssd** achieves the lowest average TRE among all methods which do not use any prior knowledge from segmentation, and the average TRE compared to the methods with masks is not statistically significant (p-value>0.05) in most of the presented cases.

	TRE (avg ± std) [in *mm*]						
		without mask prior				with mask prior	
#	before	iso- **ssd**	ani- **ssd**	ibil- **ssd**	abil- **ssd**	lg- **ssd**	mm- **ssd**
c1	3.89±2.7	1.08±0.6	1.08±0.6	1.05±0.5	1.08±0.6	1.08±0.6	1.07±0.6
c2	4.34±3.9	1.11±0.6	1.10±0.6	1.08±0.6	1.10±0.6	1.09±0.6	1.08±0.6
c3	6.94±4.0	1.51±0.9	1.50±0.9	1.46±0.9	1.49±0.9	1.47±0.9	1.47±0.9
c4	9.83±4.8	2.21±1.8	2.19±1.7	2.05±1.5	2.18±1.7	2.14±1.6	2.09±1.5
c5	7.48±5.5	2.21±1.9	2.16±1.8	2.02±1.7	2.08±1.7	2.03±1.7	2.03±1.7
c6	10.9±6.9	2.98±2.6	2.82±2.4	2.48±1.8	2.71±2.2	2.35±1.6	2.34±1.6
c7	11.0±7.4	3.58±3.5	3.42±3.3	2.78±2.3	3.25±3.1	2.47±1.7	2.49±1.7
c8	15.0±9.0	7.62±8.5	7.13±8.1	3.96±3.8	6.35±7.3	3.92±3.6	4.19±4.2
c9	7.92±3.9	2.29±1.7	2.21±1.6	1.89±1.2	2.08±1.4	1.84±1.0	2.58±1.7
c10	7.30±6.3	2.56±3.1	2.54±3.1	2.35±2.5	2.48±3.0	2.09±2.1	2.09±2.0
mean[*]	8.46±5.4	2.71±1.9	2.61±1.8	**2.11±0.9**	2.48±1.5	2.05±0.8	2.14±0.9

[*] mean over 10 cases

shown in Fig. 4 also indicates that providing a good image descriptor can help to improve the plausibility of estimated deformation field. As can be seen, the NGF-based Demons slightly decreases the amount of smoothing between lungs and the mediastinum,thus enhances a limited level of sliding.

4.5. Quantification of sliding motion

An additional experiment was conducted to quantify the locations and level of detected sliding motion of the presented framework. In order to analyse such discontinuous motion, we use a sliding motion measure recently proposed in literature (Amelon et al., 2013) which calculates the maximum shear stretch γ_{max} of the estimated deformation field. It was shown that γ_{max} characterises sliding in the lung based only on the displacement field obtained from the registration of CT data (Amelon et al., 2013). The maximum shear stretch of the deformation field is defined as follows:

$$\gamma_{max} = \frac{\gamma_1 - \gamma_3}{2} \tag{10}$$

where γ_1 and γ_3 are the maximal and minimal principal stretch components, respectively, obtained from eigenvalue decomposition of the deformation field gradients.

We calculate γ_{max} for all the voxels of the estimated deformation fields with the results for case *c5* from the *Dir-Lab* data set shown in Fig. 6 (in a natural

Table 3: Average target Registration Error (TRE) and standard deviation obtained for the Dir-Lab data set using the NGF Demons with four different filtering kernels (between 3rd (**iso-ngf** and 6th column (**abil-ngf**)) and for the Demon with the isotropic Gaussian kernel (**iso-ngf**) with two different masks (last two columns). The proposed **ibil-ngf** achieves the lowest average TRE among all methods which do not use any prior knowledge from segmentation, and the average TRE compared to the methods with masks is not statistically significant (p-value>0.05) in most of the presented cases.

	TRE (avg ± std) [in mm]						
		without mask prior				with mask prior	
#	before	iso-ngf	ani-ngf	ibil-ngf	abil-ngf	lg-ngf	mm-ngf
c1	3.89±2.7	1.08±0.6	1.10±0.6	1.05±0.6	1.11±0.6	1.08±0.6	1.06±0.6
c2	4.34±3.9	1.10±0.6	1.12±0.6	1.08±0.6	1.14±0.6	1.10±0.6	1.11±0.6
c3	6.94±4.0	1.53±0.9	1.51±0.9	1.49±0.9	1.56±0.9	1.52±0.9	1.53±0.9
c4	9.83±4.8	1.93±1.3	2.00±1.3	1.90±1.3	1.98±1.3	1.92±1.3	1.98±1.4
c5	7.48±5.5	2.04±1.7	2.05±1.7	1.99±1.7	2.10±1.7	2.03±1.7	2.02±1.7
c6	10.9±6.9	2.69±1.9	2.46±2.0	2.36±1.9	2.41±1.9	2.30±1.8	2.56±1.9
c7	11.0±7.4	2.78±2.4	2.56±2.1	2.32±1.9	2.32±1.9	2.25±1.8	2.27±1.7
c8	15.0±9.0	6.04±6.6	6.25±7.7	3.58±3.4	4.54±5.6	3.50±3.1	3.88±4.3
c9	7.92±3.9	2.03±1.1	1.90±1.3	1.74±1.0	1.80±1.1	1.78±1.1	1.80±1.1
c10	7.30±6.3	2.27±2.2	2.20±2.7	2.02±2.1	1.94±1.8	1.91±1.8	2.10±2.0
mean[*]	8.46±5.4	2.35±1.4	2.31±1.5	**1.95±0.7**	2.09±1.0	1.93±0.7	2.06±0.8

[*] mean over 10 cases

logarithmic scale). The visual inspection of the coronal plane of the maximum shear stretch obtained for the deformation field from **ibil-dem** shows very high values of γ_{max} at the pleural cavity boundaries $\gamma_{max} \gg 5$, especially at the inferior part of lungs (depicted by red arrows), while the region of the superior part of the lungs was found to be fixed (depicted by red arrows). We selected the maximum shear stretch of the deformation field $\gamma_{max} = 5$ as a noticeable level of sliding motion based on the conclusion given in Amelon et al. (2013), where $\gamma_{max} = 5$ indicates the amount of interlobar sliding for control subject. The axial plane indicates more sliding at the dorsal than at the ventral part of the body. For comparison, the results for **iso-ssd** show a relatively small amount of sliding at the lung boundaries (with $\gamma_{max} < 5$) thus confirming that diffusion regularisation (performed by a Gaussian smoothing of displacement fields) does not preserve motion discontinuities. Although in the entire chest cage and abdomen registration the sliding motion at the pleural cavity boundaries is more prominent, minor sliding motion patterns could be observed inside the lungs (around fissures). This may suggest that sliding between lung lobes could potentially be estimated using the proposed registration framework, however very accurate segmentations of the lung lobes need to obtained to correlate such little level of motion. Similarly, a minor sliding motion is also noticeable near the diaphragm which could indicate presence of motion between the liver and lungs interfaces. Sliding motion of the liver was recently investigated by Pace et al. (2013), but these results did not confirm the superiority of registration

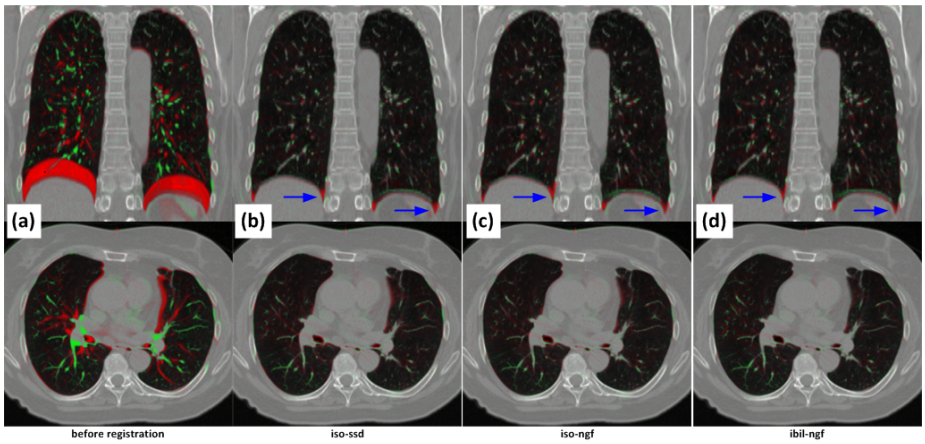

Figure 3: Qualitative registration results for case $c5$ of the Dir-Lab data set. The top row shows a coronal view of the reference image with the corresponding overlap of exhale image (red and green) while the bottom row shows an axial view. In columns from left to right: (a) before registration; (b) Demons with isotropic Gaussian kernel (**iso-ssd**), (c) NGF-based Demons with isotropic Gaussian kernel (**iso-ngf**), (d) the proposed NGF-based Demons with supplementary bilateral kernels (**ibil-ngf**). While all methods produce visually similar outcomes, registration using **ibil-ngf** slightly improves registration accuracy especially close to the lung boundary (depicted by corresponding blue arrows).

with explicit sliding motion estimation for this application.

4.6. Comparison to other methods using the Dir-Lab data set

The comparison to the state-of-the-art algorithms, presented in this section, is performed with respect to the average target registration error between 300 landmarks identified for each of ten maximum inhale and exhale volumes from the publicly available *Dir-Lab* data set (Castillo et al., 2009). This comparison is done by quotation of the reported TRE, not by direct evaluation of these methods.

The approaches that require some preprocessing steps to enable sliding motion modelling are as follows. Schmidt-Richberg et al. (2012b) reported the results for three cases of a presented variational approach: with the direction dependent regularisation (DDR) which was particularly designed to handle sliding motion of lungs (TRE=$2.13 \pm 1.8mm$), without this form of regularisation (TRE=$3.02 \pm 2.8mm$), and with lung masks (TRE=$1.99 \pm 1.6mm$). Recently, Schmidt-Richberg et al. (2012a) presented an improved version of the DDR with a fast explicit diffusion (FED) registration model, where the TRE was further reduced to $1.55 \pm 1.1mm$. The resulting TRE for a registration with a locally adaptive regularisation based on anisotropic diffusion presented in (Pace et al., 2013) is $3.71 \pm 4.1mm$ with further significant improvement of the TRE=$2.78 \pm 3.0mm$ for a version explicitly implementing sliding motion. The evaluation of the classic B-Spline registration (Rueckert et al., 1999) for the *Dir-Lab* data was presented by Delmon et al. (2013) for which it achieved

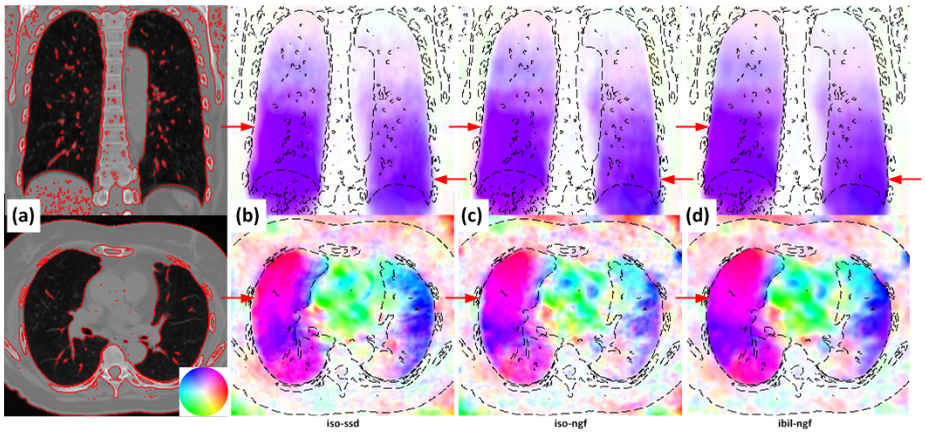

Figure 4: Visual analysis of registration results for case $c5$ of the Dir-Lab data set: The top row shows a coronal view, and the bottom row shows an axial view of the colour coded representation of deformation field vectors (in HSV colour space). In columns from left to right: (a) the coronal and axial view of the reference image with the corresponding contour shown for visual guidance (solid red or dashed black line); (b) Demons with isotropic Gaussian kernel (**iso-ssd**), (c) NGF-based Demons with isotropic Gaussian kernel (**iso-ngf**), (d) the proposed NGF-based Demons with supplementary bilateral kernels (**ibil-ngf**). Registration using **ibil-ngf** yields a smooth deformation field inside the pleura cavity whilst successfully preserving sliding motion at the lung boundary (compare corresponding red arrows in the regions of interest).

a TRE of $4.5 \pm 2.6mm$, whilst a multi-region B-Spline registration with an explicit sliding motion modelling utilising the motion masks (mentioned in Sec. 4.2) achieved a TRE of $1.7 \pm 0.3mm$. The lowest TRE reported recently in the literature on that data, to the best knowledge of the authors, was presented by Rühaak et al. (2013) and has a TRE=$0.99 \pm 1.1mm$. These results were achieved using the lung masks (the same masks as evaluated for the isotropic Demon in our comparison, denoted by **lg**), and with an additional affine preregistration for the binary images of the segmented structures before performing the intensity-driven deformable registration. The best registration algorithm from the recent EMPIRE10 challenge (Murphy et al., 2011), a symmetric, diffeomorphic, demons-like gsyn algorithm from the ANTS package (Avants et al., 2008), obtained a TRE=$2.43 \pm 4.1mm$ for non-masked evaluation for the *Dir-Lab* data set, and a TRE=$1.57 \pm 2.1mm$ for evaluation including segmented lung tissue only (the results are taken from (Heinrich et al., 2013)). A very comprehensive comparison of various implementations of Demon registrations for the lung segmented data was reported by Gu et al. (2010). The only five cases were evaluated (the cases denoted here by $c1$ to $c5$) and the average TRE for the best performing method (so-called adjusted double force (ADF) Demon) was $1.51 \pm 1.46mm$, while **ibil-ngf** for the cases denoted by $c1$ to $c5$ achieves $1.50 \pm 0.44mm$.

Contrary to the above approaches, Heinrich et al. (2013) presented an MRF-based, discrete-optimisation framework with an implicit sliding motion preserva-

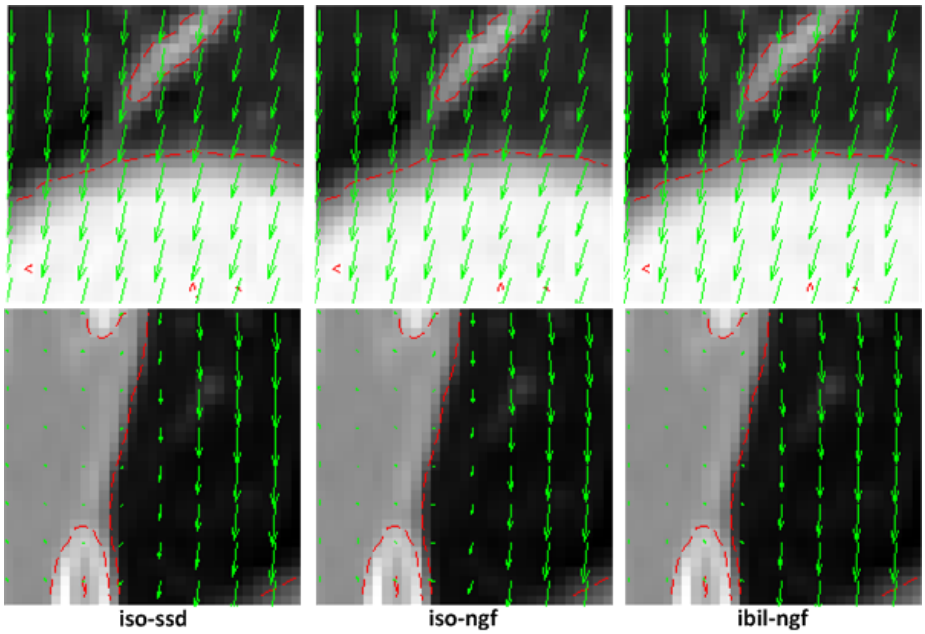

Figure 5: Representative patches of the estimated displacement field (represented by green arrows) for case $c5$ of the Dir-Lab data set. The top row shows that the proposed method (**ibil-ngf**) is capable of estimating smooth displacements at the lung and abdomen interface (similar to the methods with Gaussian smoothing). The bottom row shows that the Demons registration with Gaussian smoothing (**iso-ssd**) underestimates motion close to the pleural cavity boundary, while the proposed algorithm (**ibil-ngf**) recovers more uniform lung motion with clear sliding. Registration using bilateral filtering based regularisation yields smooth deformation inside the pleura cavity whilst preserving sliding motion at the lung boundary.

tion model and a simultaneously estimated ventilation map during registration that also does not require a prior segmentation. This method achieved a TRE of $1.43 \pm 1.3mm$ for the *Dir-Lab* data.

Summarising, the proposed registration framework yields considerable better results (TRE=$1.95 \pm 0.8mm$) than the majority of the aforementioned approaches with a locally anisotropic diffusion regularisation or other implementations of masked/unmasked version of Demons even if such are supported by some preregistration processing (segmentation of sliding structures or sliding motion detection).

5. Discussion and Conclusions

The proposed regularisation framework is related to the recent works presented by Schmidt-Richberg et al. (2012b) and Pace et al. (2013), where a locally adaptive anisotropic diffusion based regularisation was also proposed. However, those methodologies require some preprocessing steps *i.e.* segmentation of the lung mask to restrict smoothing to the normal direction of the segmented object,

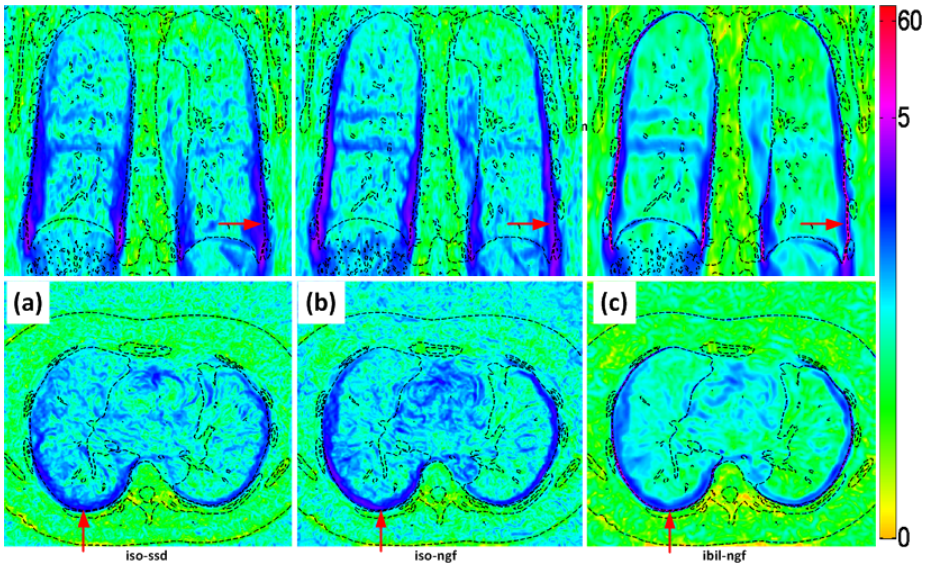

Figure 6: Quantification of sliding motion for case $c5$ of the Dir-Lab data set. The top row shows the coronal (dorsal) view of the maximal shear stretch γ_{max} (in a logarithmic scale) while the bottom row shows the axial view for: (a) Demons with isotropic Gaussian kernel (**iso-ssd**), (b) NGF-based Demons with isotropic Gaussian kernel (**iso-ngf**), (c) the proposed NGF-based Demons with supplementary bilateral kernels (**ibil-ngf**). It can be easily observed that the proposed regularization model preserves sliding motion at the lung boundaries, which is exhibited by high values of γ_{max}, while classic Demons smoothes the displacement field (and by this γ_{max}) across the lung boundaries (depicted by red arrows).

thus performing explicit modelling of sliding motion. To avoid the requirement of an initial segmentation, Schmidt-Richberg et al. (2012b) proposed an extended version of this algorithm with automatic detection of sliding organs. In contrast to these approaches, in our framework the detection of sliding organs is implicitly incorporated in the supplementary smoothing kernels. Similarly, a tissue dependent filtering of deformation fields was also investigated by Staring et al. (2007). While that approach was used to penalize deformation of rigid structures in the body, our methodology more naturally filters each structure based on its local intensities and motion properties.

The proposed methodology of filtering the deformation field using bilateral filter kernels could also be directly applied to the updates of deformation fields instead of the deformation fields. This however was not investigated in this study because *using diffusion based regularisation requires less computational resources than fluid regularisation for similar level of smoothness* (Risser et al., 2013). Meanwhile, very smooth displacement fields were found to characterise plausibility of inner thoracic cage motion (Schmidt-Richberg et al., 2012b)

Employing an anisotropic diffusion kernel G_{ani} based on the local image structure tensors D Eq. (4) for bilateral filtering of the deformation field of the *Dir-Lab* data set, does not improve the overall registration accuracy when

compared to the isotropic Gaussian kernel (TRE for **ibil-dem** and **abil-dem** was $2.11mm$ and $2.48mm$, respectively, and **ibil-ngf** and **abil-ngf** was $1.95mm$ and $2.09mm$ respectively). Such behaviour of the anisotropic diffusion kernel could be expected as the isotropic bilateral filtering already introduces spatial anisotropy, and it also suggests that the isotropic Gaussian kernel enhanced additionally by two other kernels (G_r and $G_{\vec{u}}$) already sufficiently represents the plausible properties of the estimated deformation fields. Furthermore, this observation is consistent with the conclusion given in (Schmidt-Richberg et al., 2012b) that the inner pleural cavity motion remains very smooth and standard isotropic regularisation performs in these regions very reasonably. Moreover, this can be supported by the results reported in our experimental section. Applying the Demons framework for segmented CT volumes (**lg-dem** and **mm-dem**), without explicit discontinuous field estimation, demonstrates very good performance. Correspondingly, the results from the NCAT data set where both isotropic and anisotropic kernels achieved similar performance, could be explained by the validation criterion (DICE) used for the presented accuracy assessment. For the *Dir-Lab* data set, we used the manually selected, well-populated landmarks, whereas the NCAT data set was assessed by somewhat more global measures i.e. segmentation labels of relatively large organs. Thus, any more subtle differences between those methods could not be further quantified (Rohlfing, 2012).

The normalised gradient field image representation incorporated in the presented framework offers relatively low computational requirements, and easily extends the usability of the Demons framework for some multi-modal registration tasks. An interesting prospective work of the presented NGF Demons registration framework would be to use it for other vector-valued image descriptors such as a modality independent neighbourhood descriptor (MIND) (Heinrich et al., 2012). We also plan to evaluate a recently proposed LCC-Demons (Lorenzi et al., 2013) (which is based on the local correlation coefficient) linked with our proposed regularisation scheme in order to assess its robustness to local intensity changes of lung tissue.

From a technical point of view, the current implementation has one considerable limitation i.e. a substantial amount of computational time is required (naturally dependent on volume size, and number of iterations). This is due to a convolution based filtering methodology applied to filter deformation fields at each iteration. On average using our non-optimised multi-threaded Matlab/C++ code on standard CPU, the registration for Dir-Lab data sets using the SSD-based Demons with the isotropic bilateral filtering procedure (ibil-ssd) takes around 60 minutes, while the NGF-based Demons with the isotropic bilateral filtering procedure (ibil-ngf) takes around 75 minutes. The registration approach using anisotropic bilateral filtering for the deformation field filtering takes about 30% longer. However, the procedure of bilateral filtering can be implemented using more efficient algorithms using e.g. an approximated version of kernels (for a comprehensive review see Paris et al. (2007)) or a recently proposed recursive version (Yang, 2012), therefore can still be improved in terms of computational performance. Additionally the Demons framework due to

its voxel independent processing, is well-suited for an efficient parallel implementation, thus overall algorithm performance could be improved (Gu et al., 2010). Furthermore, following (Sand and Teller, 2008) to speed up the presented methodology, the use of bilateral filtering of the deformation field could be restricted to the regions and their close neighbourhoods of the displacement field discontinuities.

To summarise, in this paper, we have presented an extension to the commonly used Demons registration framework that efficiently handles discontinuities of displacement fields to allow estimation of sliding motion. To consider that different organs can have various motion patterns including aforementioned sliding motion of the lungs during the respiratory cycle, we use a locally adaptive regularisation model that implicitly distinguishes these motion differences based on the spatial smoothness, and local changes of intensities and deformation fields. Most importantly, in contrast to the majority of current state-of-the art studies, no prior knowledge (e.g. using from lung segmentations) was used to guide the regularisation during the registration.

Our presented regularisation model marks a novel contribution to the field of sliding organ registration. We performed an extensive validation of the presented registration framework and compared it against the state-of-the-art deformation field filtering techniques. An average TRE of $1.95 \pm 0.7mm$ was found for a challenging *Dir-Lab* respiratory data set, which clearly demonstrates the advantage of the presented regularisation model. The registration accuracy of the proposed approach compares well with previously published results on the same data sets. Additionally, we also incorporated the squared differences between the normalized gradient fields of the input images as a similarity measure driving Demons registration. The results suggests that the NGF-based Demons registration successfully addresses a problem of local intensity changes due to air compression during breathing. A quantitative analysis shown in this paper indicates that masking intensities outside the lungs can substantially increase the registration accuracy within the lungs, however it requires an additional segmentation step that has to be carefully prepared. Furthermore, such methods do not recover the plausible deformation in the whole image domain (except approaches where registration is performed for each segmented region separately and then merged into one piece-wise continuous deformation field). Thus, applications where our approach seems to be promising include longitudinal lung diseases studies or treatment adjustment in image-guided radiotherapy, particularly for cases where disease or tumour develops changes close to the chest wall boundaries. Importantly, we also used a numerical criterion, the maximum shear stretch of estimated deformation field, to localise and quantify the ability of the proposed framework to estimate sliding motion. The presented results show that our method is capable of preserving sliding motion at the lung boundaries in an effective manner.

Future work will focus on registration of structural and functional imaging data such as PET/CT analysis (Baluwala et al., 2013), where statistical similarity measures such as mutual information, correlation ratio (Hermosillo et al., 2002; Zikic et al., 2011) or local correlation coefficient (Lorenzi et al.,

2013) may need to be used, and therefore, an efficient and reliable regularisation model will be even more important to preserve medical plausibility of the estimated deformation field. While our focus in this paper was on validation of the presented methodology for lung motion data analysis, another interesting direction could be addressed such as an investigation of the performance of the proposed methodology when applied to scans of a different organ e.g. for liver motion estimation, where sliding motion also occurs (Xie et al., 2011), or for CT/cone beam CT (CBCT) registration without the need of correcting intensity changes (Nithiananthan et al., 2011).

Acknowledgement

We would like to acknowledge funding from the CRUK/EPSRC Cancer Imaging Centre at Oxford. JAS and LR also wish to acknowledge the INSMI-CNRS/John Fell Oxford University Press (OUP) Research Fund.

Amelon, R.E., Cao, K., Reinhardt, J.M., Christensen, G.E., Raghavan, M.L., 2013. A measure for characterizing sliding on lung boundaries. Annals of Biomedical Engineering , 1–9.

Avants, B.B., Epstein, C.L., Grossman, M., Gee, J.C., 2008. Symmetric diffeomorphic image registration with cross-correlation: evaluating automated labeling of elderly and neurodegenerative brain. Medical Image Analysis 12, 26–41.

Baluwala, H.Y., Risser, L., Schnabel, J.A., Saddi, K.A., 2013. Toward physiologically motivated registration of diagnostic CT and PET/CT of lung volumes. Medical Physics 40, 021903.

Beg, M.F., Miller, M.I., Trouvé, A., Younes, L., 2005. Computing large deformation metric mappings via geodesic flows of diffeomorphisms. International Journal of Computer Vision 61, 139–157.

Castillo, R., Castillo, E., Guerra, R., Johnson, V., McPhail, T., Garg, A., Guerrero, T., 2009. A framework for evaluation of deformable image registration spatial accuracy using large landmark point sets. Physics in Medicine and Biology 54, 1849–1870.

Castillo, R., Castillo, E., Martinez, J., Guerrero, T., 2010. Ventilation from four-dimensional computed tomography: density versus Jacobian methods. Physics in Medicine and Biology 55, 4661–4685.

Delmon, V., Rit, S., Pinho, R., Sarrut, D., 2013. Registration of sliding objects using direction dependent B-splines decomposition. Physics in Medicine and Biology 58, 1303–1314.

Ding, K., Cao, K., Fuld, M.K., Du, K., Christensen, G.E., Hoffman, E.A., Reinhardt, J.M., 2012. Comparison of image registration based measures

of regional lung ventilation from dynamic spiral CT with Xe-CT. Medical Physics 39, 5084–5098.

Ehrhardt, J., Werner, R., Schmidt-Richberg, A., Handels, H., 2011. Statistical modeling of 4D respiratory lung motion using diffeomorphic image registration. IEEE Transactions on Medical Imaging 30, 251–265.

Gorbunova, V., Sporring, J., Lo, P., Loeve, M., Tiddens, H.A., Nielsen, M., Dirksen, A., de Bruijne, M., 2012. Mass preserving image registration for lung CT. Medical Image Analysis 16, 786–795.

Gu, X., Pan, H., Liang, Y., Castillo, R., Yang, D., Choi, D., Castillo, E., Majumdar, A., Guerrero, T., Jiang, S.B., 2010. Implementation and evaluation of various demons deformable image registration algorithms on a GPU. Physics in Medicine and Biology 55, 207–219.

Haber, E., Modersitzki, J., 2006. Intensity gradient based registration and fusion of multi-modal images, in: International Conference on Medical Image Computing and Computer Assisted Intervention (MICCAI), Springer Berlin Heidelberg. pp. 726–733.

Haber, E., Modersitzki, J., 2007. Image registration with guaranteed displacement regularity. International Journal of Computer Vision 71, 361–372.

Heinrich, M.P., Jenkinson, M., Bhushan, M., Matin, T., Gleeson, F.V., Brady, M., Schnabel, J.A., 2012. MIND: Modality independent neighbourhood descriptor for multi-modal deformable registration. Medical Image Analysis 16, 1423–1435.

Heinrich, M.P., Jenkinson, M., Brady, M., Schnabel, J.A., 2010. Discontinuity preserving regularisation for variational optical-flow registration using the modified Lp norm, in: Medical Image Analysis for the Clinic - A Grand Challenge, Workshop MICCAI, pp. 185–194.

Heinrich, M.P., Jenkinson, M., Brady, M., Schnabel, J.A., 2013. MRF-based deformable registration and ventilation estimation of lung CT. IEEE Transactions on Medical Imaging 32, 1239–1248.

Hermosillo, G., Chefd'Hotel, C., Faugeras, O., 2002. Variational methods for multimodal image matching. International Journal of Computer Vision 50, 329–343.

Lassen, B., Kuhnigk, J.M., Schmidt, M., Krass, S., Peitgen, H.O., 2011. Lung and lung lobe segmentation methods at Fraunhofer MEVIS, in: Fourth International Workshop on Pulmonary Image Analysis, pp. 185–200.

Lorenzi, M., Ayache, N., Frisoni, G.B., Pennec, X., , A.D.N.I., 2013. LCC-Demons: a robust and accurate symmetric diffeomorphic registration algorithm. Neuroimage 81, 470–483.

Mansi, T., Pennec, X., Sermesant, M., Delingette, H., Ayache, N., 2011. iLogDemons: A demons-based registration algorithm for tracking incompressible elastic biological tissues. International Journal of Computer Vision 92, 92–111.

Modersitzki, J., 2004. Numerical Methods for Image Registration. Oxford University Press.

Murphy, K., Van Ginneken, B., Reinhardt, J.M., Kabus, S., Ding, K., Deng, X., Cao, K., Du, K., Christensen, G.E., Garcia, V., et al., 2011. Evaluation of registration methods on thoracic CT: The EMPIRE10 challenge. IEEE Transactions on Medical Imaging 30, 1901–1920.

Nithiananthan, S., Schafer, S., Uneri, A., Mirota, D.J., Stayman, J.W., Zbijewski, W., Brock, K.K., Daly, M.J., Chan, H., Irish, J.C., et al., 2011. Demons deformable registration of CT and cone-beam CT using an iterative intensity matching approach. Medical Physics 38, 1785.

Pace, D., Aylward, S., Niethammer, M., 2013. A locally adaptive regularization based on anisotropic diffusion for deformable image registration of sliding organs. IEEE Transactions on Medical Imaging 32, 2114–2126.

Papiez, B.W., Heinrich, M.P., Risser, L., Schnabel, J.A., 2013. Complex lung motion estimation via adaptive bilateral filtering of the deformation field, in: International Conference on Medical Image Computing and Computer Assisted Intervention (MICCAI), Springer-Verlag Berlin Heidelberg. pp. 25–32.

Paris, S., Kornprobst, P., Tumblin, J., Durand, F., 2007. A gentle introduction to bilateral filtering and its applications, in: ACM SIGGRAPH 2007 courses, ACM. p. 1.

Peyrat, J.M., Delingette, H., Sermesant, M., Xu, C., Ayache, N., 2010. Registration of 4D cardiac CT sequences under trajectory constraints with multichannel diffeomorphic Demons. IEEE Transactions on Medical Imaging 29, 1351–1368.

Risser, L., Vialard, F.X., Baluwala, H.Y., Schnabel, J.A., 2013. Piecewise-diffeomorphic image registration: Application to the motion estimation between 3D CT lung images with sliding conditions. Medical Image Analysis 17, 182–193.

Rohlfing, T., 2012. Image similarity and tissue overlaps as surrogates for image registration accuracy: widely used but unreliable. IEEE Transactions on Medical Imaging 31, 153–163.

Ruan, D., Esedoglu, S., Fessler, J.A., 2009. Discriminative sliding preserving regularization in medical image registration, in: IEEE International Symposium on Biomedical Imaging: From Nano to Macro, 2009. ISBI '09., pp. 430–433.

Rueckert, D., Sonoda, L.I., Hayes, C., Hill, D.L.G., Leach, M.O., Hawkes, D.J., 1999. Non-rigid registration using free-form deformations: Application to breast mr images. IEEE Transactions on Medical Imaging 18, 712–721.

Rühaak, J., Heldmann, S., Kipshagen, T., Fischer, B., 2013. Highly accurate fast lung CT registration, in: SPIE Medical Imaging, International Society for Optics and Photonics. pp. 86690Y–86690Y.

Sand, P., Teller, S., 2008. Particle video: Long-range motion estimation using point trajectories. International Journal of Computer Vision 80, 72–91.

Sarrut, D., 2006. Deformable registration for image-guided radiation therapy. Medical Physics 16, 285–297.

Schmidt-Richberg, A., Ehrhardt, J., Werner, R., Handels, H., 2012a. Fast explicit diffusion for registration with direction-dependent regularization, in: Dawant, B.M., Christensen, G.E., Fitzpatrick, J.M., Rueckert, D. (Eds.), 5th International Workshop on Biomedical Image Registration (WBIR), Springer-Verlag Berlin Heidelberg. pp. 220–228.

Schmidt-Richberg, A., Werner, R., Handels, H., Ehrhardt, J., 2012b. Estimation of slipping organ motion by registration with direction-dependent regularization. Medical Image Analysis 16, 150–159.

Segars, W.P., 2001. Development and application of the new dynamic NURBS-based cardiac-torso (NCAT) phantom. Ph.D. thesis. University of North Carolina.

Staring, M., Klein, S., Pluim, J.P.W., 2007. Nonrigid registration with tissue-dependent filtering of the deformation field. Physics in Medicine and Biology 52, 6879–6892.

Thirion, J.P., 1998. Image matching as a diffusion process: an analogy with Maxwell's demons. Medical Image Analysis 2, 243–260.

Tomasi, C., Manduchi, R., 1998. Bilateral filtering for gray and color images, in: Procedings of the Sixth International Conference on Computer Vision (ICCV-98), pp. 839–846.

Tschumperle, D., Deriche, R., 2005. Vector-valued image regularization with PDEs: A common framework for different applications. IEEE Transactions on Pattern Analysis and Machine Intelligence 27, 506–517.

Vandemeulebroucke, J., Bernard, O., Rit, S., Kybic, J., Clarysse, P., Sarrut, D., 2012. Automated segmentation of a motion mask to preserve sliding motion in deformable registration of thoracic CT. Medical Physics 39, 1006.

Vercauteren, T., Pennec, X., Perchant, A., Ayache, N., 2009. Diffeomorphic Demons: Efficient non-parametric image registration. NeuroImage 45, S61–S72.

Weickert, J., Romeny, B.T.H., Viergever, M.A., 1998. Efficient and reliable schemes for nonlinear diffusion filtering. IEEE Transactions on Image Processing 7, 398–410.

Weiss, E., Wijesooriya, K., Dill, S.V., Keall, P.J., 2007. Tumor and normal tissue motion in the thorax during respiration: Analysis of volumetric and positional variations using 4d ct. International Journal of Radiation Oncology, Biology, Physics 67, 296–307.

Wu, Z., Rietzel, E., Boldea, V., Sarrut, D., Sharp, G.C., 2008. Evaluation of deformable registration of patient lung 4DCT with subanatomical region segmentations. Medical Physics 35, 775–781.

Xiao, J., Cheng, H., Sawhney, H., Rao, C., Isnardi, M., 2006. Bilateral filtering-based optical flow estimation with occlusion detection, in: Computer Vision ECCV 2006, Springer Berlin Heidelberg. pp. 211–224.

Xie, Y., Chao, M., Xiong, G., 2011. Deformable image registration of liver with consideration of lung sliding motion. Medical Physics 38, 5351–5361.

Xing, L., Thorndyke, B., Schreibmann, E., Yang, Y., Li, T.F., Kim, G.Y., Luxton, G., Koong, A., 2006. Overview of image-guided radiation therapy. Medical Dosimetry 31, 91–112.

Yang, Q., 2012. Recursive bilateral filtering, in: Computer Vision–ECCV 2012. Springer, pp. 399–413.

Yin, Y., Hoffman, E.A., Lin, C.L., 2009. Mass preserving nonrigid registration of CT lung images using cubic B-spline. Medical Physics 36, 4213–4222.

Zikic, D., Baust, M., Kamen, A., Navab, N., 2011. A general preconditioning scheme for difference measures in deformable registration, in: Proc. IEEE International Conference on Computer Vision (ICCV), pp. 49–56.

Zimmer, H., Bruhn, A., Weickert, J., 2011. Optic flow in harmony. International Journal of Computer Vision 93, 368–388.